Micellar self-assembly, bridging and gelling behaviour of two reverse triblock poly(butylene oxide)-poly(ethylene oxide)-poly(butylene oxide) copolymers with lengthy hydrophilic bl...

ARTICLE *in* RSC ADVANCES · OCTOBER 2014

Impact Factor: 3.84 · DOI: 10.1039/C4RA10176F

THE JOURNAL OF PHYSICAL CHEMISTRY B

Article

pubs.acs.org/JPCB

Complex Self-Assembly of Reverse Poly(butylene oxide)-Poly(ethylene oxide)-Poly(butylene oxide) Triblock Copolymers with Long Hydrophobic and Extremely Lengthy Hydrophilic Blocks

Adriana Cambón,[†,∥] Edgar Figueroa-Ochoa,[‡,∥] Josué Juárez,[§] Eva Villar-Álvarez,[†] Alberto Pardo,[†] Silvia Barbosa,*[,†] J. F. Armando Soltero,[‡] Pablo Taboada,[†] and Víctor Mosquera[†]

[†]Departamento de Física de la Materia Condensada, Grupo de Física de Coloides y Polímeros, 15782-Santiago de Compostela, Spain

[‡]Laboratorio de Reología, Departamento de Ingeniería Química, CUCEI, Universidad de Guadalajara, Bolv. M. García Barragán 44430, Jalisco, México

[§]Departamento de Física, Universidad de Sonora, Rosales y Transversal, 83000 Hermosillo, Sonora, México

ABSTRACT: Amphiphilic block copolymers have emerged during last years as a fascinating substrate material to develop micellar nanocontainers able to solubilize, protect, transport, and release under external or internal stimuli different classes of cargos to diseased cells or tissues. However, this class of materials can also induce biologically relevant actions, which complement the therapeutic activity of their cargo molecules through their mutual interactions with biologically relevant entities (cellular membranes, proteins, organelles...); these interactions at the same time, are regulated by the nature, conformation, and state of the copolymeric chains. For these reasons, in this paper we investigated the self-assembly process and physico-chemcial properties of two reverse triblock poly(butylene oxide)-poly(ethylene oxide)-poly(butylene oxide) block copolymers, $BO_{14}EO_{378}BO_{14}$ and $BO_{21}EO_{385}BO_{21}$, which have been recently found to be very useful as drug delivery nanovehicles and biological response modifiers under certain conditions (A. Cambón et al. *Int. J. Pharm.* **2013**, 445, 47−57) in order to obtain a clear picture of the solution behavior of this class or block copolymers and to understand their biological activity. These block copolymers are characterized by possessing long BO blocks and extremely lengthy central EO ones, which provide them with a rich rheological behavior characterized by the formation of flowerlike micelles with sizes ranging from 20 to 40 nm in aqueous solution and the presence of intermicellar bridging even at low copolymers concentrations as denoted by atomic force microscopy. Bridging is also clearly observed by analyzing the rheological response of these block copolymers both storage and loss moduli upon changes on time, temperature, and or concentration. Strikingly, the relatively wide Poisson distribution of the polymeric chains make the present copolymers behave rather distinctly to conventional associative thickeners. The observed rich rheological behavior and their tunability also make these copolymers promising materials to configure drug gelling depots.

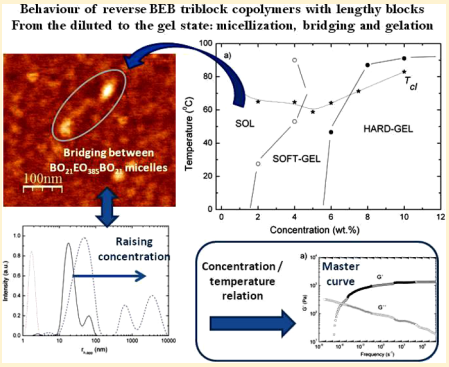

INTRODUCTION

In the last two decades, a great effort has been made through the development of a series of nanosized therapeutic products able to solubilize hydrophobic drugs, allow their sustained release, improve their pharmacokinetics, and facilitate their access to the site of action.[1−5] The properties of amphiphilic copolymers combining hydrophilic poly(ethylene oxide) units with different types of hydrophobic blocks have been found to show suitable characteristics to fulfill the former requirements (i.e., they can spontaneously self-assemble into nanoscopic core−shell micellar structures in which the core serves as a reservoir for the hydrophobic cargo, while the corona is in direct contact with the biological milieu providing "stealthiness" to evade scavenging by the mononuclear phagocyte system), which results in larger circulation times and passive accumulation in solid tumors by the enhanced permeation and retention (EPR) effect.[6] Copolymers, which combine poly(oxyethylene) and poly(oxypropylene) [EO = oxyethylene, OCH_2CH_2 and PO = oxypropylene, $OCH_2CH(CH_3)$] in a triblock structure, either direct, $EO_mPO_nEO_m$, or reverse, $PO_nEO_mPO_n$ (where the subscripts m and n denote number-average block lengths) have been the most extensively studied due to their commercial availability in a very broad range of compositions, a fair solubilization capacity and sustained release, a good biocompatibility of most varieties, and approval of some varieties by regulatory agencies to be used in pharmaceutical formulations and medical devices.[7−9] Nevertheless, $EO_mPO_nEO_m$ or $PO_nEO_mPO_n$ block copolymers possess several drawbacks. For example, the oxyanionic polymerization of propylene oxide is not straightforward, the problem lying in the transfer reaction originated from hydrogen abstraction rather than addition.[10] For example, $EO_mPO_nEO_m$

Received: January 14, 2014
Revised: April 15, 2014

   dx.doi.org/10.1021/jp500426k | *J. Phys. Chem. B* XXXX, XXX, XXX−XXX

copolymers often have a diblock component, detected as a pronounced shoulder on the high-elution-volume side of their gel permeation chromatographic curves, which leads to variation in micellization[11,12] behavior from batch to batch. In addition, there exists an incomplete micellization of the unimers, which usually leads to self-assembled nanostructures with limited drug solubilization ability and stability upon dilution in the bloodstream.

To circumvent these problems, during the past few years a series of more hydrophobic block copolymer counterparts with similar architecture but with the PO segment replaced by a more hydrophobic one such as poly(butylene oxide) (PBO), poly(styrene oxide) (PSO), or phenylglycidyl ether (PG) have been proposed with the aim of improving the solubilization capacities, release profiles, and the rheological properties of the polymeric micelles for poorly water-soluble drugs.[13−19]

Special attention has been paid to copolymers with 1,2-butylene oxide (BO) as the hydrophobic monomer. Transfer is not a problem in the laboratory polymerization of BO,[20] but this monomer (as PO does) adds to the growing chain to give a secondary oxyanion; also, the slow initiation of EO chains at the secondary termination may lead to a broadened EO-block-length distribution.[21] However, this effect is eliminated if BO blocks are polymerized last when forming EO_mBO_m diblock and $BO_nEO_mBO_n$ triblock copolymers. Reverse $BO_nEO_mBO_n$ triblock copolymers have potential for the control of rheological properties in aqueous systems, particularly as associative thickeners, thanks to the formation of transient micelle clusters or networks by bridging of extended chains between micelles as previously observed, for example, in copolymer $BO_{10}EO_{410}BO_{10}$.[22−24] The larger relative hydrophobicity of the BO block compared to PO (6-fold as estimated from the ratio of the logarithms of the molar critical micellar concentrations, cmc)[16] enables the formation of polymeric micelles at much lower copolymer concentrations and subsequent larger solubilized drug concentrations in the micelle core, providing excellent properties as drug delivery nanocarriers.[25] In addition, these copolymers were demonstrated to be "biologically active" in the sense of, for example, enhancing drug toxicity to cancerous cells by inhibiting the P-glycoprotein P efflux pump mechanism.[25] Nevertheless, a complete and detailed physicochemical characterization of the former class copolymers is still lacking, which might help to obtain a better understanding of their behavior as biologically response modifiers and to open up new potential applications as injectable drug gelling depots.

Hence, in this work we present a deep characterization of the self-assembly process and the physicochemical properties of copolymers $BO_{14}EO_{378}BO_{14}$ and $BO_{21}EO_{385}BO_{21}$ by different techniques such as static and dynamic light scattering (SLS and DLS, respectively), transmission electron microscopy (TEM), atomic force microscopy (AFM), and rheometry. Both copolymers possess much longer BO blocks than previously analyzed $BO_nEO_mBO_n$ copolymers. This enabled us to observe the effects of both the collapse of longer BO blocks in solution of reverse copolymeric structures and the splitting of BO units number between two blocks, especially in dilute solution since the range of hydrophobicity has been greatly restricted for these copolymers (i.e., from BO_4 to BO_{12}, 8 to 24 BO units per molecule).[16]

2. EXPERIMENTAL SECTION

2.1. Materials. Copolymers were prepared by oxyanionic polymerization of dry 1,2-butylene oxide initiated by poly(ethylene glycol) monomer of different molecular weights activated by mixing with KOH and heating while stirring under vacuum (70 °C, 0.1 mmHg, 100 h) to remove water. Vacuum line and ampule techniques served to exclude moisture. Gel permeation chromatography (GPC) was used to characterize the distribution widths of the products as the ratio of mass-average to number-average molar mass (i.e., M_w/M_n) by using a Waters GPC system equipped with a 1515 isocratic pump and a 2410 refractive index detector (Waters, Milford, MA). Chloroform was used as the eluent, and monodisperse PEO was employed as the standard. ^{13}C NMR spectra recorded on a Bruker ARX400 spectrometer (Bruker, Milton, ON, Canada) in deuterated chloroform were used to obtain absolute values of block length and composition and to verify block architecture. The general methods used have been described previously in detail.[22,26] Table 1 summarizes the molecular characteristics of the copolymers.

Table 1. Molecular Characteristics of the Copolymers

polymers	M_n (g/mol)[a]	M_w/M_n[b]	M_w (g/mol)	cmc (g/dm^3)[c]
$BO_{14}EO_{378}BO_{14}$	18 600	1.12	20 830	0.058
$BO_{21}EO_{385}BO_{21}$	20 000	1.10	22 000	0.025

[a]Estimated by NMR. [b]Estimated by GPC; M_w calculated from M_n and M_w/M_n. Estimated uncertainty: M_n to ±3%; M_w/M_n to ±0.01. [c]Values from ref 27.

2.2. Dynamic and Static Light Scattering (DLS and SLS). SLS intensities were measured by means of an ALV-5000F (ALV-GmbH, Germany) instrument with vertically polarized incident light (λ = 488 nm) supplied by a diode-pumped Nd:YAG solid-state laser (Coherent Inc., CA) and operated at 2 W and combined with an ALV SP-86 digital correlator with a sampling time of 25 ns to 100 ms (for DLS). Measurements were made at an angle of $\theta = 90°$ to the incident beam, as appropriate for particles smaller than the light wavelength. The intensity scale was calibrated against scattering from toluene. Solutions were filtered through Millipore Millex filters (Triton free, 0.22 μm porosity) directly into cleaned scattering cells and allowed to equilibrate at the requested temperature for 10 min before measurement. Each experiment was repeated at least three times. Sampling time was 5−10 min for each run in order to define an optimal correlation function. For DLS, the correlation functions were analyzed by the CONTIN method to obtain the intensity distributions of decay rates (Γ).[28] From the decay rate distributions, the apparent diffusion coefficients [$D_{app} = \Gamma/q^2$, $q = (4\pi n_s/\lambda)\sin(\theta/2)$] were derived, with n_s as the solvent refractive index. Values of the apparent hydrodynamic radius ($r_{h,app}$, radius of the hydrodynamically equivalent hard sphere corresponding to D_{app}) were calculated from the Stokes−Einstein equation:

$$r_{h,app} = kT/(6\pi\eta D_{app}) \quad (1)$$

where k is the Boltzmann constant and η is the viscosity of water.

2.3. Transmission Electron Microscopy (TEM). Micellar solutions of both copolymers were applied dropped over carbon-coated copper grids, blotted, washed, negatively stained with 2 wt % phosphotungstic acid, air-dried, and then examined

dx.doi.org/10.1021/jp500426k | J. Phys. Chem. B XXXX, XXX, XXX−XXX

with a Phillips CM-12 transmission electron microscope operating at an accelerating voltage of 120 kV.

2.4. Clouding. Copolymer solutions were prepared by weighting the required amount of each copolymer followed by the addition of the same volume of cold water (1 mL). Copolymer solutions were homogenized under stirring at low temperature before being stored at least for 1 day (T ~ 4 °C) to ensure complete dissolution. Clouding temperatures (T_{cl}) were determined by slowly heating (0.2 °C min^{-1}) the copolymer solutions from 0 to 90 °C by both visual inspection and detection of the transmitted light through solutions by means of a UV−vis spectrophotometer equipped with a temperature control Peltier device and a multicell sample holder (Cary 100, Agilent, Germany). A plot of transmitted intensity versus temperature was obtained. The cloud point was determined as the midpoint of an abrupt decrease in the transmitted light intensity from a plot of transmitted intensity versus temperature, as previously described.[24]

2.5. Rheometry. Solutions were prepared by weighting copolymer and deionized water into small tubes and subsequent mixing in the mobile state before being stored for a day or more at low temperature (ca. 5 °C). Rheological characterization was carried out using a controlled stress AR2000 rheometer (TA Instruments, DE) with Peltier temperature control. Samples were investigated using cone−plate geometry (cone diameter 40 mm, angle 0.5°) and a solvent trap to maintain a water-saturated atmosphere around the sample cell to avoid evaporation. The temperature dependence of storage (G) and loss (G'') moduli was measured either by temperature scans at frequency f = 1 Hz and heating rates of 1 °C min^{-1} or by frequency scans at several temperatures (1−80 °C). Experiments were carried out in an oscillatory shear mode, with the strain amplitude (A) maintained at a low value (A < 0.5%) by means of the autostress facility of the software. This ensured that measurements of G' and G'' were in the linear viscoelastic region. A dynamic time sweep test under A = 0.5% and f = 1 Hz was performed before each frequency scan at a fixed temperature to ensure that the sample truly reached the equilibrium state.

2.6. Atomic Force Microscopy (AFM). AFM images of block copolymer solutions were performed on freshly cleaved mica substrates. The measurements were performed in a JEOL instrument (model JSPM 4210) in noncontact mode using nitride cantilevers NSC15 from MicroMasch (typical working frequency and spring constant of 325 kHz and 40 N/m, respectively). The AFM samples were dried in air or under a nitrogen flow when required. Control samples (freshly cleaved mica and buffer solution) were also investigated to exclude possible artifacts. Topography and phase-shift data were collected in the trace and retrace direction of the raster, respectively. The offset point was adapted accordingly to the roughness of the sample. The scan size was usually 500 nm (aspect ratio, 1 × 1), with a sample line of 256 points and a step size of 1 μm. The scan rate was tuned proportionally to the area scanned and kept within the 0.35−2 Hz range. Each sample was imaged several times at different locations on the substrate to ensure reproducibility. Diameters and heights of copolymer aggregates were determined by sectional analysis taken from the average of several sections through the aggregates.

3. RESULTS AND DISCUSSION

3.1. Clouding. The clouding and phase behavior of $BO_nEO_mBO_n$ copolymers is not completely resolved yet due to the unavailability of a full range of block lengths. To fill this gap, clouding temperatures (T_{cl}) were first determined for solutions of copolymers $BO_{14}EO_{378}BO_{14}$ and $BO_{21}EO_{385}BO_{21}$ in the concentration range of 0.1−10 wt % by visual inspection and UV−vis spectroscopy following the methodology of Zhou et al.[24] A good agreement was observed between both methods. Figure 1 shows T_{cl} as a function of copolymer concentration. In

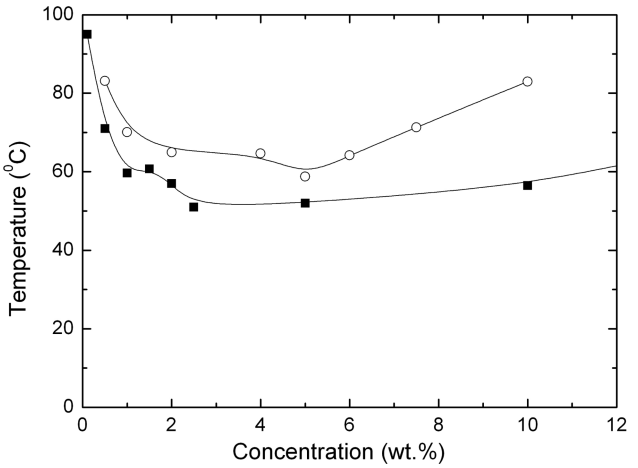

Figure 1. Clouding temperatures for copolymers $BO_{14}EO_{378}BO_{14}$ (○) and $BO_{21}EO_{385}BO_{21}$ (■) obtained by UV−vis spectroscopy. The lines were drawn to guide the eye.

the one-phase region, the cmc values were previously found to be below 0.1 mg/mL for both copolymers.[27] Hence, the cloud point behavior can represent the phase transition of a copolymer micellar solution which phase separates ca. 20 °C above T_{cl}. In general, copolymer $BO_{21}EO_{385}BO_{21}$ displayed lower T_{cl} than $BO_{14}EO_{378}BO_{14}$, as expected for its longer hydrophobic blocks. For $BO_{14}EO_{378}BO_{14}$, the cloud-point profile exhibited a shallow minimum at 5 wt % (at 60 °C), while for $BO_{21}EO_{385}BO_{21}$ this minimum was observed at 3 wt % (at 51 °C); for both copolymers T_{cl} starts again to increase at larger concentrations. High T_{cl} coincident with gel formation have also been observed in related systems (i.e., aqueous solutions of copolymers $BO_{12}EO_{114}BO_{12}$ and $BO_{12}EO_{227}BO_{12}$).[23,29,30] Liu et al.[31] have investigated the effect of EO and BO block lengths on T_{cl} of 1 wt % solutions of $BO_nEO_mBO_n$ copolymers bearing short EO (m < 40) and BO (n < 7) blocks. These authors showed that T_{cl} decreased with increases in BO-block length at a constant EO-block one, and it increased with an increase in EO-block length at a constant BO-block one. The results reported here confirm that Liús conclusions can be also applied to longer copolymers and higher concentrations (i.e., T_{cl} is lower the most hydrophobic the copolymer is). However, in the present case the copolymers' behavior is largely influenced by their extremely long EO-blocks which causes T_{cl} to increase if compared to structurally related $BO_{12}EO_{114}BO_{12}$, $BO_{12}EO_{227}BO_{12}$, or $BO_{10}EO_{410}BO_{10}$ copolymers previously studied.[22,32]

3.2. Population Size Distributions. DLS measurements of $BO_{14}EO_{378}BO_{14}$ and $BO_{21}EO_{385}BO_{21}$ micellar solutions at different concentrations were carried out at 10 and 25 °C. Selected intensity fraction distributions of log $r_{h,app}$ ($r_{h,app}$ being the apparent hydrodynamic radius) are illustrated in Figure 2a for copolymer $BO_{21}EO_{385}BO_{21}$ at 25 °C as an example. For c < cmc, the population distributions obtained show only a single peak attributed to singly dispersed copolymer chains ($r_{h,app}$ =

dx.doi.org/10.1021/jp500426k | J. Phys. Chem. B XXXX, XXX, XXX−XXX

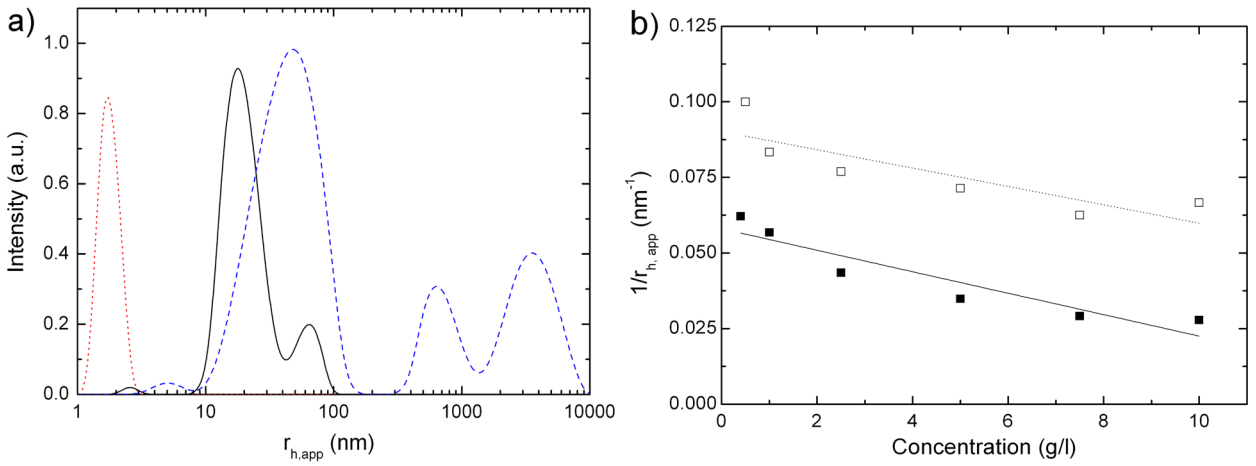

Figure 2. (a) Intensity-weighted population distributions obtained by DLS for copolymer $BO_{21}EO_{385}BO_{21}$ in solution at 25 °C (red, black, and blue lines correspond to 0.4, 2.5, and 10 mg/mL solutions, respectively). (b) Reciprocal apparent hydrodynamic radius, $1/r_{h,app}$, against concentration for copolymer $BO_{21}EO_{385}BO_{21}$ at 10 °C (□) and 25 °C (■).

2−3 nm) (Figure 2a, red line). It is conceivable that under these conditions the present copolymers can arrange the unimers in the form of unimolecular micelles in order to prevent the contact of BO blocks with water, thanks to the flexibility of the central, very long EO block. The low micellization enthalpy values previously derived from isothermal titration calorimetry (ITC) would confirm the tight packing of BO blocks in the unimer state so that their hydrophobic interaction with water would be really small.[27] At c > cmc, several peaks are observed in the intensity-fraction population distributions, which can correspond to unimers ($r_{h,app}$ = 2−3 nm), flowerlike micelles ($r_{h,app}$ = ca. 8 to 20 nm), and micelle clusters formed by micellar bridgening ($r_{h,app}$ = 40−60 nm) (Figure 2a, black line). Owing to the special chain architecture of $BO_nEO_mBO_n$-type block copolymers, the formation of flowerlike micelles would involve bending of EO blocks while keeping the two terminal BO blocks in the same micellar core (an entropy-loss process). Another possibility might be that the two BO blocks in one polymer chain would reside in two adjacent micelles, and the EO block would be used as a bridge. This kind of cross-linking among the micelles can finally promote an open network structure (the so-called micellar clusters), reflected in the DLS population distributions (Figure 2a, blue line). Peaks corresponding to unimers and micelles were single narrow peaks, while those belonging to micellar clusters were broader. As the concentration increased, the latter peak became more intense, denoting larger cluster sizes. Population distributions also slightly shifted to smaller sizes as the temperature decreases (not shown). This was as expected provided that water becomes a better solvent for micelles as the temperature is lowered and, hence, micellar bridging (and, hence, clustering) is reduced. On the other hand, the shape of micelles was nearly spherical as observed by TEM and AFM, with their diameters (ca., 27 ± 4 and 32 ± 5 nm for $BO_{14}EO_{378}BO_{14}$ and $BO_{21}EO_{385}BO_{21}$ as calculated from TEM, respectively) in fair agreement with those obtained from DLS data despite the usual dehydration of the copolymer corona and subsequent shrinking of the copolymer structure upon solvent evaporation during sample preparation (see Figure 3a). From AFM images, the protrusion of the EO corona can also be observed, showing a slightly less spherical micellar shape than in TEM images (Figure 3b).

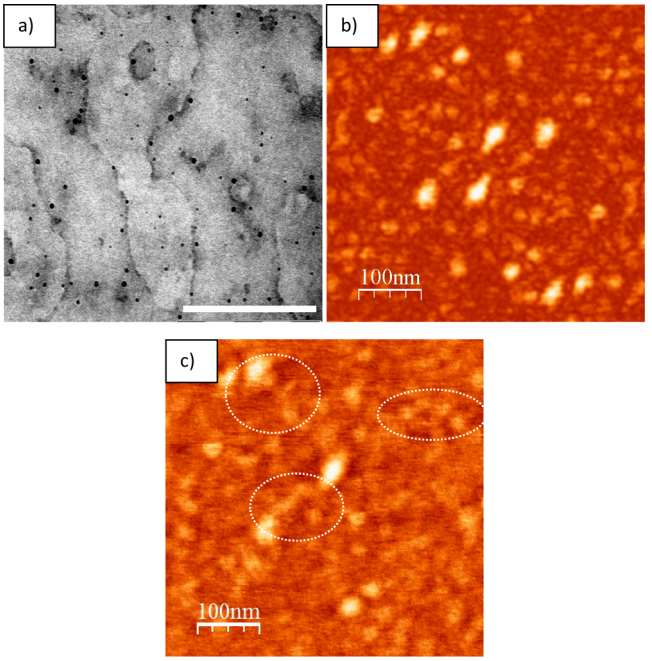

Figure 3. (a) TEM image of micelles formed by copolymer $BO_{21}EO_{385}BO_{21}$ (scale bar 500 nm); (b) AFM image of $BO_{21}EO_{385}BO_{21}$ micelles with a protruded corona; and (c) AFM image showing interchain bridges between copolymer micelles.

From plots of $1/r_{h,app}$ against copolymer concentration, the micellar hydrodynamic radii (r_h) was obtained as the intercept of each curve at c = 0 (see Figure 2b and Table 2). $1/r_{h,app}$ is proportional to the apparent diffusion coefficient, D_{app}, but

Table 2. Micellar Parameters of Copolymers $BO_{14}EO_{378}BO_{14}$ and $BO_{21}EO_{385}BO_{21}$.[a]

copolymer	T (°C)	10^5 M_W (g/mol)	r_h (nm)	N_W
$BO_{14}EO_{378}BO_{14}$	10	2.5	8.4	13
	25	3.4	18.5	18
$BO_{21}EO_{385}BO_{21}$	10	1.7	11.1	8
	25	1.8	20.4	9

[a]Estimated uncertainty in M_w and r_h: ± 5%.

dx.doi.org/10.1021/jp500426k | J. Phys. Chem. B XXXX, XXX, XXX−XXX

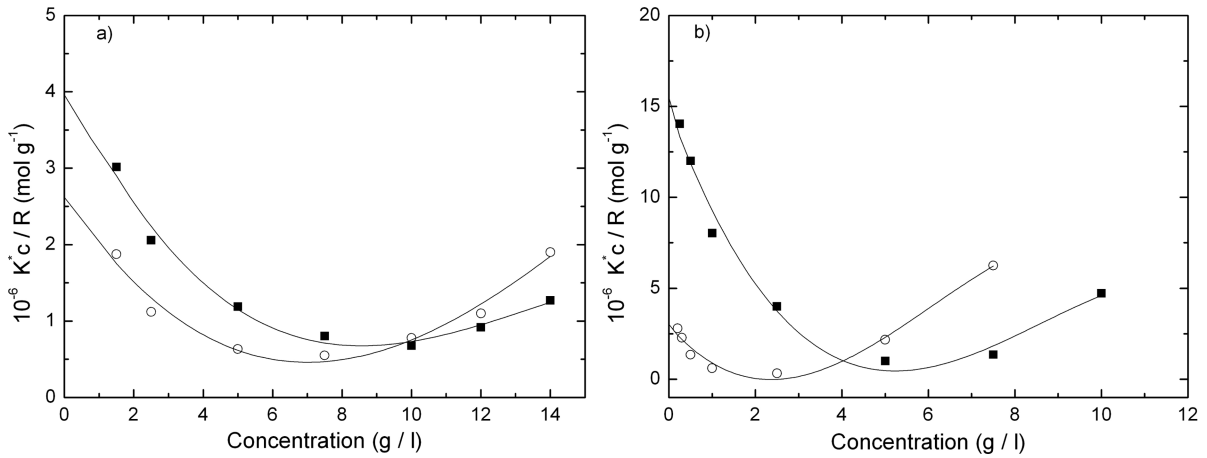

Figure 4. Debye plots for $BO_{14}EO_{378}BO_{14}$ (○) and $BO_{21}EO_{385}BO_{21}$ (■) copolymers at (a) 10 °C and (b) 25 °C.

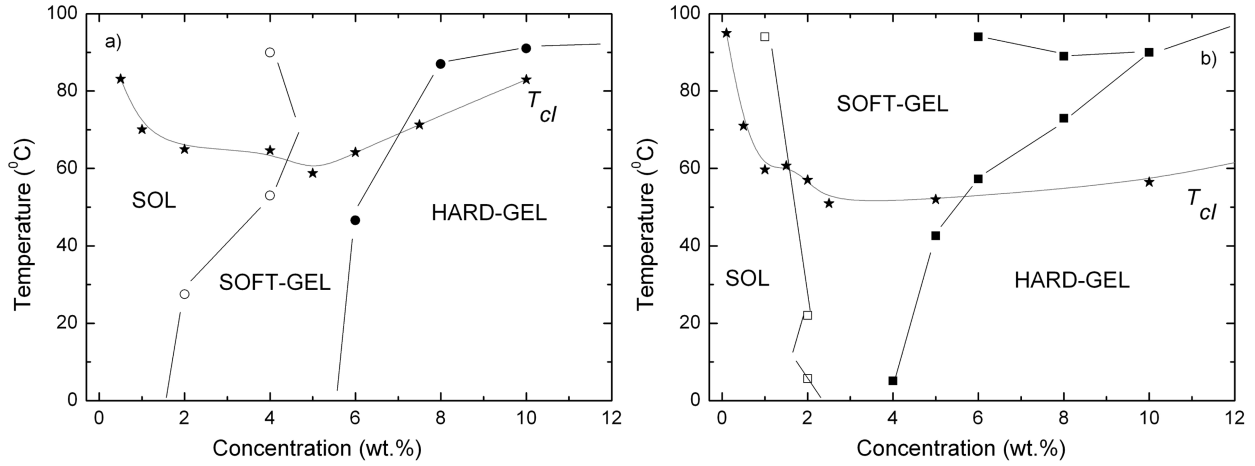

Figure 5. Phase diagrams delined using tube inversion and rheometry data from temperature scans. (a) corresponds to $BO_{14}EO_{378}BO_{14}$ and (b) to $BO_{21}EO_{385}BO_{21}$. (○) corresponds to the sol-soft gel transition, (■) denotes the soft gel-hard gel one, and (★) the clouding temperature. Lines were drawn to guide the eye.

without the influence of temperature and solution viscosity. The negative slopes of these plots pointed to negative values of the second virial (A_2) coefficient; this indicates that micelles interact attractively by bridging,[33] as confirmed by the protrusions observed from some micelles to others denoting intermicellar bridging in AFM images (Figure 3c). Van der Waals attraction and polymer depletion should not play significant roles in the present dilute micellar systems.[24,26]

Both the BO and EO block lengths will affect intermicellar interactions: longer BO-end blocks should imply that intermicellar interaction can become stronger, while long central EO blocks can make the BO blocks extend into the solution more easily.[34] Comparison of the present data with those previously reported for shorter $BO_mEO_nBO_m$ copolymers suggested that $BO_{14}EO_{378}BO_{14}$ and $BO_{21}EO_{385}BO_{21}$ displayed a stronger intermicellar attraction as would correspond to reverse copolymers with relatively long BO blocks and extremely lengthy EO ones.

3.3. Micellar Properties. Since the hydrodynamic radii of the present polymeric micelles (Table 2) are small compared to the light wavelength, intraparticle interference can be neglected. Clustering at higher copolymer concentrations changes this picture, but here we focused on the behavior in the dilute regime. Debye plots, for instance, plots based on

$$\frac{K^*c}{I - I_s} = \frac{1}{M_w^m} + 2A_2c + \cdots \quad (2)$$

where I is the light scattering intensity from solution relative to that from toluene, I_s is the corresponding quantity for the solvent, c is the concentration (in g dm^{-3}), M_w^m is the mass-average molar mass of the solute, A_2 the second virial coefficient, and K^* the appropriate optical constant for $BO_{14}EO_{378}BO_{14}$ and $BO_{21}EO_{385}BO_{21}$ at 10 and 25 °C, are shown in Figure 4. K^* includes the specific refractive index increment (dn/dc), whose insensitiveness to composition in $BO_nEO_mBO_n$ systems is already known (dn/dc = 0.135 cm^3/g).[26] Although at low concentrations the present copolymers should tend to loop in isolated micelles, there is a finite probability of bridging because the system is in dynamic equilibrium as corroborated previously by AFM images, which implies an attractive intermicellar interaction. In particular, the upturns in the Debye plots at low concentrations would be caused by both the micelle-molecule equilibrium (i.e., the dissociation of micelles at concentrations approaching the cmc) and the existence of attractive interactions due to bridging, even at such low concentrations (c < 5 mg/mL). At larger concentrations, repulsive interactions (effectively a hard-sphere interaction) are increasingly dominant, giving rise to large positive slopes in the Debye plots. However, in the present case

dx.doi.org/10.1021/jp500426k | J. Phys. Chem. B XXXX, XXX, XXX−XXX

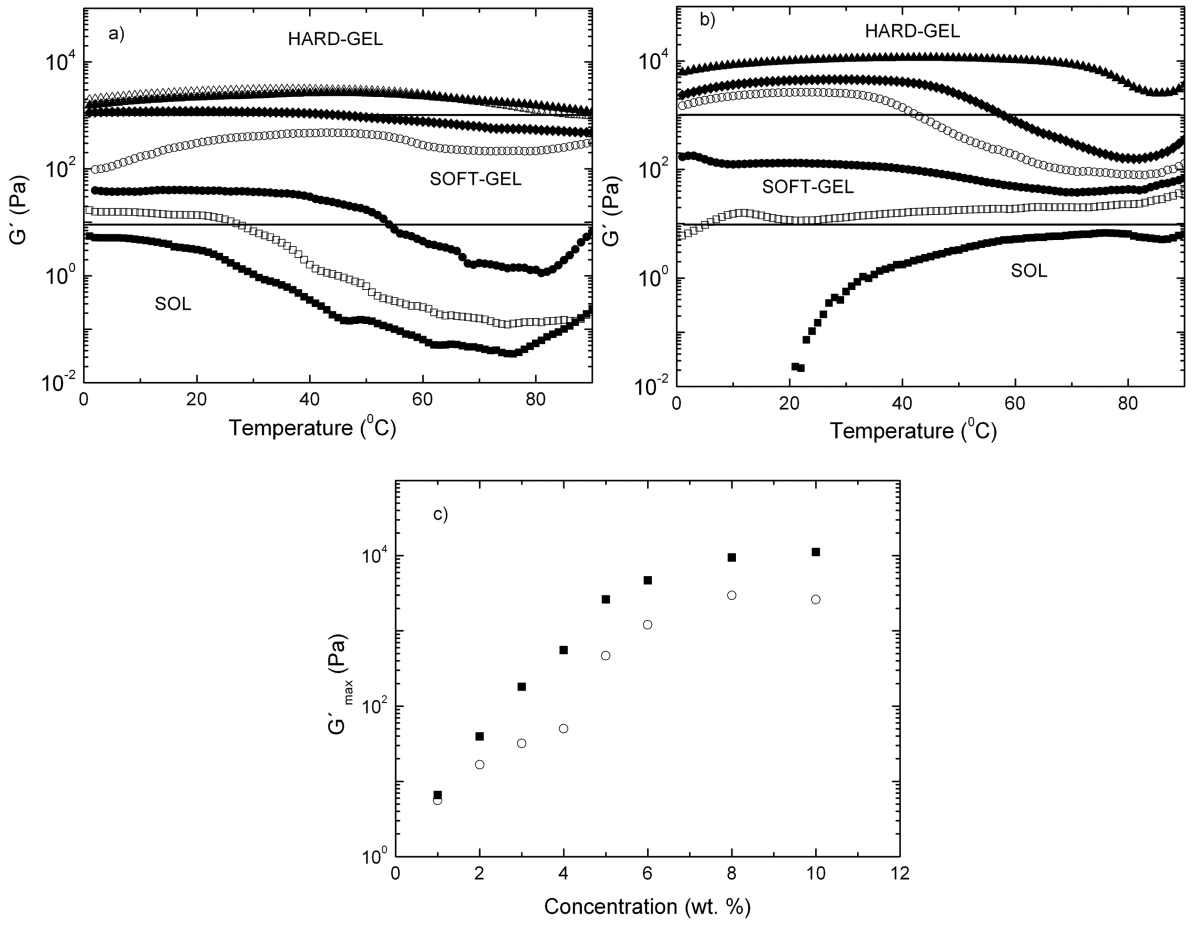

Figure 6. Temperature scans in the range of 1−90 °C of log (G') at f = 1 Hz for copolymers (a) $BO_{14}EO_{378}BO_{14}$ and (b) $BO_{21}EO_{385}BO_{21}$. The concentrations analyzed for copolymer $BO_{14}EO_{378}BO_{14}$ were (■) 1, (□) 2, (●) 4, (○) 5, (◆) 6, (▲) 8, and (△) 10 wt %, while (■) 1, (□) 2, (●) 3, (○) 5, (◆) 6 and (▲) 10 wt % for $BO_{21}EO_{385}BO_{21}$. (c) Plots of G'_{max} against concentration for copolymers (○) $BO_{14}EO_{378}BO_{14}$ and (■) $BO_{21}EO_{385}BO_{21}$.

attractive interactions due to intermicellar bridging also play an important role counterbalancing the effect of repulsive interactions, as denoted by the small observed positive slopes of Debye plots (see Figure 4) in the concentration range analyzed. Bridging is also observed to increase by raising the solution temperature. Water becomes a better solvent at low temperatures and a more-solvated EO-block corona involves a larger excluded volume of one micelle to another, as observed from steeper slopes at high copolymer concentrations at 10 °C.

Values of M_w^m were obtained by linear extrapolation of experimental data at c < 0.5 wt % and calculated from $N_w = M_w^m/M_w$ (Table 2). Association numbers for copolymer $BO_{21}EO_{385}BO_{21}$ were larger than those of $BO_{14}EO_{378}BO_{14}$ as corresponds to a copolymer with a larger hydrophobic core and stronger intermicellar interactions. Also, N_w values for these copolymers slightly increased as the temperature rose, provided that water becomes a poorer solvent for the polyoxyethylene blocks.[13] The present N_w values were also larger than those previously obtained for the $BO_{10}EO_{410}BO_{10}$ copolymer as corresponds to copolymers with longer BO blocks and similar to those of $BO_{10}EO_{271}BO_{10}$ or $BO_{12}EO_{260}BO_{12}$,[24,34] with much shorter EO blocks. In the latter cases, the increment of N_w due to the presence of longer BO blocks in the present copolymers was counterbalanced by the N_w reduction expected by their longer EO blocks, as observed for other pol(oxyalkylene) copolymers.[16]

3.4. Rheological Behavior. *3.4.1. Tube Inversion.* Tube inversion was used to obtain a preliminary definition of the mobile−immobile regions of the phase diagrams. For copolymer $BO_{14}EO_{378}BO_{14}$, a mobile viscous fluid is present up to a concentration of 5 wt %, while an immobile gel is formed above (Figure 5a). The gel phase progressively converts into a very viscous fluid, resembling a high-temperature boundary, in the range from 40 to 90 °C, depending on concentration: the higher the concentration, the larger the boundary temperature. In the case of copolymer $BO_{21}EO_{385}BO_{21}$, a relatively mobile fluid is observed at concentrations below 4 wt % and 15 °C. From such temperature and above, the formation of a more viscous fluid took place, possibly as a consequence of micellar bridging (Figure 5b). Above 4 wt %, a transparent immobile gel is observed. Nevertheless, it is worth mentioning that the characterization of solutions containing these two triblock copolymers was complicated above ca. 3 wt % by the tube-inversion method by the relatively important viscosity of the fluids, no doubt a result of micellar bridging, which made accurate detection of fluid/gel boundaries by this method difficult. Whereas fluid/gel boundaries in solutions of EO_mBO_n and $EO_mBO_nEO_m$ diblock copolymers can be readily detected to ±1 °C, those in the present system could only be detected to ±4 °C. Hence, to ensure the boundaries of the phase diagrams, rheometry measurements were also performed.

dx.doi.org/10.1021/jp500426k | J. Phys. Chem. B XXXX, XXX, XXX−XXX

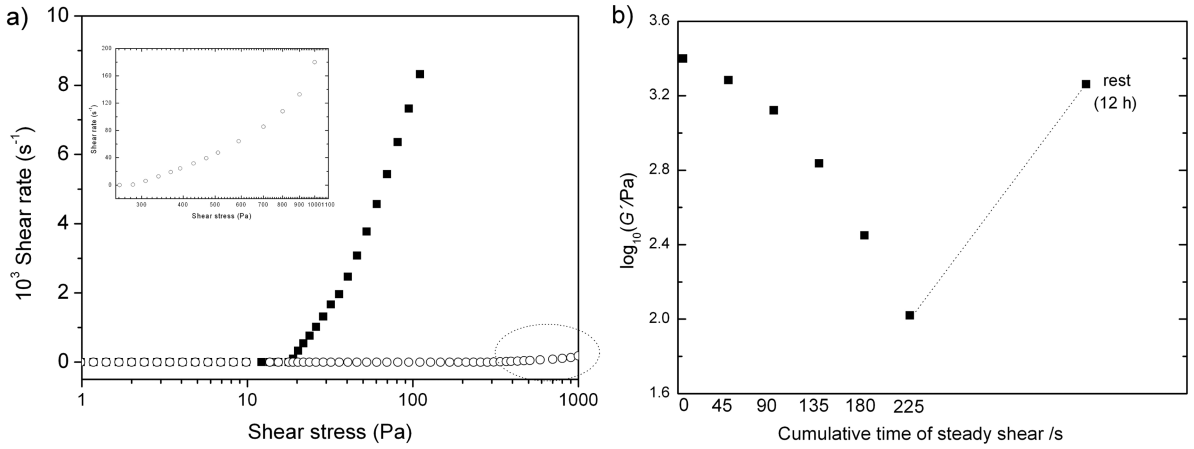

Figure 7. (a) Yield stresses under continuous shear for 3 and 10 wt % solutions of copolymer $BO_{14}EO_{378}BO_{14}$ at 20 °C. The inset shows the yield of the 10 wt % solution in greater detail. (b) Dynamic moduli measurement at 1 Hz and 0.5% strain amplitude after time under steady shear and after rest for a 10 wt % solution of copolymer $BO_{14}EO_{378}BO_{14}$.

3.4.2. Concentration and Temperature Dependence. Temperature scans of $\log(G')$ at f = 1 Hz for copolymers $BO_{14}EO_{378}BO_{14}$ and $BO_{21}EO_{385}BO_{21}$ in the range of 1−90 °C were performed. A view of the dependence of G' on concentration and temperature is provided by the examples shown in Figure 6. At 1 wt %, copolymer samples are unstructured fluids (sols, with G' < 10 Pa and G'' > G'). In the concentration range from 1 to 4 wt % copolymer $BO_{14}EO_{378}BO_{14}$ was a viscous complex fluid at low and room temperatures characterized by 10 < G' < 1000 Pa and G' > G'' (i.e., a soft gel adopting Hvidt's et al. notation),[35] and it became a sol at higher temperatures (45 and 53 °C at 2 and 4 wt %, respectively). The observed decrease in G' at high temperatures and, thus, the transition from a viscous fluid to a sol can be associated with a worsening solvent environment compressing the EO-block corona. At 5 wt %, the copolymer was a viscous fluid in the whole temperature range, while it became an immobile gel at larger concentrations (arbitrarily defined by G' > G'' and G' > 1000 Pa at f = 1 Hz). In particular, the copolymer was an immobile gel in the temperature range of 5 to ca. 50 °C at 6 wt % and in the whole temperature range at 8 and 10 wt %. At these concentrations, packing becomes the dominant contribution and the temperature dependence of G' resembled that found for nonbridging micellar solutions but, presumably, modified by bridging.

Since copolymer $BO_{21}EO_{385}BO_{21}$ has longer hydrophobic blocks than $BO_{14}EO_{378}BO_{14}$ and, thus, a lower cmc value, its gelification is expected to take place at lower concentrations. As observed from Figure 6b, $BO_{21}EO_{385}BO_{21}$ was a viscous fluid above 6 °C at 2 wt %, whereas at 3 and 4 wt %, it remained in such a state in the whole temperature range. At 5 and 6 wt %, this copolymer became an immobile gel below ca. 44 and 60 °C, respectively, and a viscous fluid above such temperatures. Finally, above 8 wt % the copolymer formed an immobile gel in the whole temperature range.

All the above data allowed a more exact definition of the phase diagram, as shown in Figure 5. In addition, more information could be extracted from rheology plots. At comparable concentrations, maximum values of $G'(T)$, G'_{max}, were larger for solutions of $BO_{21}EO_{385}BO_{21}$ than for $BO_{14}EO_{378}BO_{14}$ (Figure 6c). This is consistent with a stronger intermicellar bridging of the copolymer bearing longer BO blocks and the formation of micelles with a more-swollen EO-block corona, so high-exclusion volumes would favor packing at high polymer concentrations. In fact, for both copolymers, G' values increased markedly with concentration, with a predominant elastic behavior (G' > G'') in most of the temperature and concentration ranges analyzed.

In general, at concentrations above ca. 5−6 wt %, G' is observed to increase in the temperature range from 5 to ca. 50−60 °C (depending on copolymer concentration) to subsequently decrease at higher temperatures, promoting a transition from an immobile gel to a complex viscous fluid. Structural studies by SAXS and SANS of aqueous solutions of block copolymers have shown that just outside the gel phase, the fluid contains small micellar domains with the same structure as the gel phase;[36] hence, the viscous fluid after the gel phase can be characterized as a defective cubic structure, as previously observed for related EO_mBO_n and $EO_mBO_nEO_m$ copolymers.[37]

As discussed elsewhere[37] for aqueous micellar gels of copoly(oxyalkylene)s of different block architectures, the onset of gelation and the associated increase in G' with T at low temperatures is associated with an increase in the extent of micellization and, in the present case, with the extent of bridging. The observed decrease in G' at high temperatures for both copolymers can be associated with a worsening solvent environment compressing the EO-block corona and, thereby, with a decrease in the effective micellar volume fraction. The observation of peaks in G'' at the high-T boundaries of the immobile gels provides another indication of these effects.[30]

3.4.3. Steady Shear. The measurement of the yield stress (σ_y) provides a second measure of the resistance to motion under shear stress. The shear stress required to cause immobility in the tube inversion test has been previously shown to be 30−40 Pa.[38] Yield stresses were measured in particular to confirm the concentration regions at which a viscous fluid is present, that is, the point at which the shear rate departed measurably from zero. Examples are shown in Figure 7a (i.e., $\sigma_y \sim$ 20 Pa for a 3 wt % solution at 20 °C but $\sigma_y \sim$ 0 Pa for the same solution at T = 50 °C for copolymer $BO_{14}EO_{378}BO_{14}$). At higher concentrations, the yield stress was high at all temperatures (i.e., $\sigma_y \sim$ 350 Pa for a 10 wt % solution at 20 °C). There is also evidence in Figure 7a of shear thinning attributed to disruption of the structure under shear flow. The effect of steady shear was also investigated for a 6 wt

dx.doi.org/10.1021/jp500426k | J. Phys. Chem. B XXXX, XXX, XXX−XXX

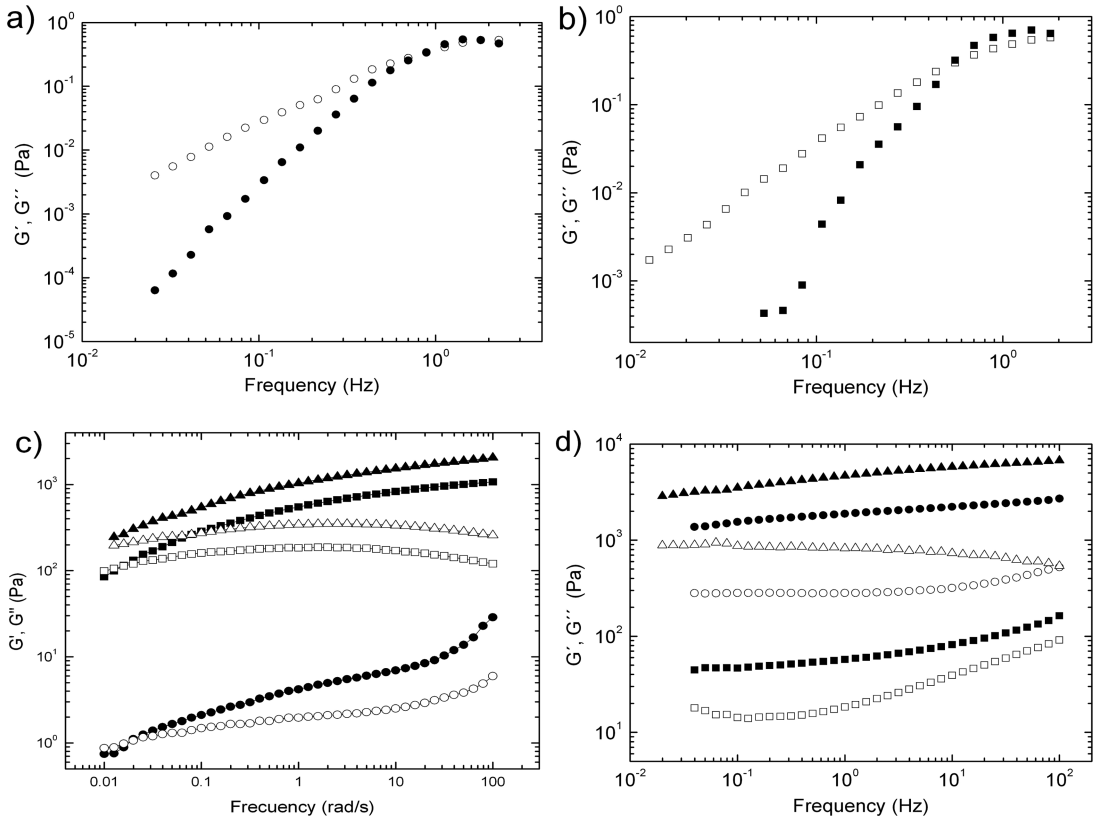

Figure 8. Frequency scans for (a) $BO_{14}EO_{378}BO_{14}$ and (b) $BO_{21}EO_{385}BO_{21}$ at 1 wt % and 10 °C. (c) $BO_{21}EO_{385}BO_{21}$ copolymer at 2 (circles), 3 (squares), and 4 wt % (triangles) at 20 °C and (d) $BO_{14}EO_{378}BO_{14}$ copolymer at 6 wt % and 20 (circles) and 60 °C (squares) and 10 wt % (triangles) at 20 °C. Filled symbols denote G', while open ones denote G''.

% solution at 30 °C, which was subjected to a steady shear stress of 500 Pa (well above the yield stress) for 45 s prior to immediate determination of modulus under the usual conditions. Then, the steady shear was immediately reapplied for subsequent periods and the determination of modulus repeated until accumulating 225 s of shear overall (Figure 7b). It was observed that moduli measured at f = 1 Hz decreased with this treatment. Resting the solution after the experiment for ca. 90 min resulted in only a small change in modulus, but resting overnight restored the modulus to, essentially, the initial G value. The 6 wt % gel at 30 °C is near to its fluid-gel transition temperature (see Figure 5), and this may allow extensive disruption of structure and lead to slow recovery, which may well be an effect of the bridged network, as also observed in some related systems.[23] This behavior is in contrast to diblock EO_mBO_n and triblock $EO_mBO_nEO_m$ copolymers, which have shown similar reductions in G' after application of large-amplitude oscillatory shears but rapid recovery (<1 min) of the modulus at rest.

3.4.4. Frequency Scans. Effects of changes in the extent of micellar bridging and packing are apparent in the different mechanical responses to the applied frequency. Hence, the frequency dependence of the moduli was determined for solutions of copolymers $BO_{14}EO_{378}BO_{14}$ and $BO_{21}EO_{385}BO_{21}$ in the concentration range of 1−10 wt %. Examples are shown in Figure 8. For example, 1 wt % solutions of copolymers $BO_{14}EO_{378}BO_{14}$ and $BO_{21}EO_{385}BO_{21}$ typically possessed values of G'' exceeding those of G' over the most accessible frequency range except at high frequencies, where a moduli crossover occurs from which a relaxation time t = 0.90 and 0.55 s, respectively, could be determined (Figure 8, panels a and b). The behavior can be approximated to that of a Maxwell element:

$$G' = (G_\infty \tau^2 \omega^2)/(1 + \tau^2 \omega^2)$$
$$G'' = (G_\infty \tau \omega)/(1 + \tau^2 \omega^2) \quad (3)$$

where G_∞ is the plateau value of G' at high frequency, τ is the relaxation time, and $\omega = 2\pi f$ (f = frequency in Hz). At all temperatures investigated, the slopes of the best straight lines through the data points were near to values of 2 (log G′) and 1 (log G″), which are expected when $\omega\tau \ll 1$ (i.e., typical of a Newtonian fluid).

At copolymer concentrations between 2 and 4 wt % at T = 10 °C, the scans obtained for both copolymers showed a more complex rheology with values of G' < 1 kPa. For example, a modulus crossover could be observed at low frequencies for $BO_{21}EO_{385}BO_{21}$ at 2 and 3 wt % corresponding to a Maxwell fluid showing, at most, a localized cubic order.[37] This effect must be a consequence of the attraction of micelles at temperatures at which water is a poor solvent for micelles and favored by micellar bridging too (Figure 8c). As the copolymer concentration was further increased, G' became progressively insensitive to frequency and consistently greater than G'' for both copolymers (see Figure 8, panels c and d). In particular, for copolymer concentrations ranging from 4 to 6 wt %, an immobile gel with relatively high G' values (>1 kPa) existed typically below 50−60 °C, depending on copolymer type and concentration. Above such temperature threshold, a viscous fluid was observed (Figure 8d). This type of viscous fluid at temperatures and concentrations relatively near the gel

dx.doi.org/10.1021/jp500426k | J. Phys. Chem. B XXXX, XXX, XXX−XXX

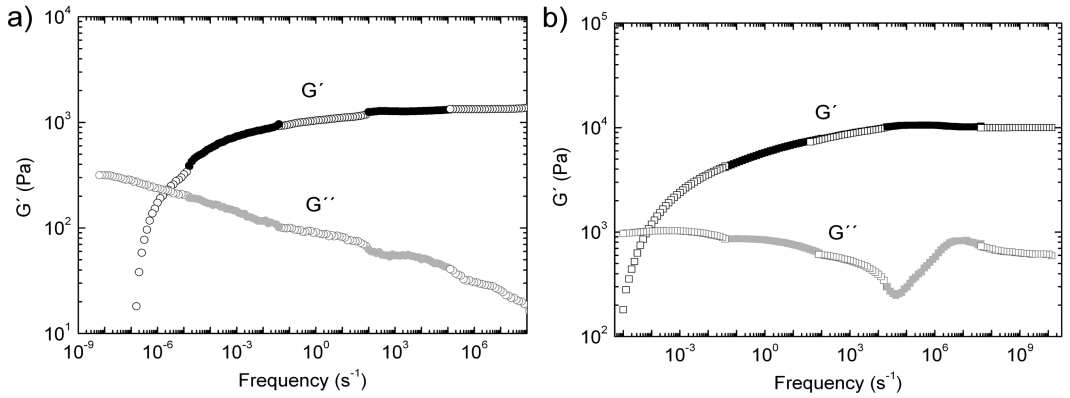

Figure 9. Master curve plots obtained for the (a) $BO_{14}EO_{378}BO_{14}$ copolymer at 6 wt % and (b) $BO_{21}EO_{385}BO_{21}$ copolymer at 10 wt % (reference temperature, T_0 = 30 °C).

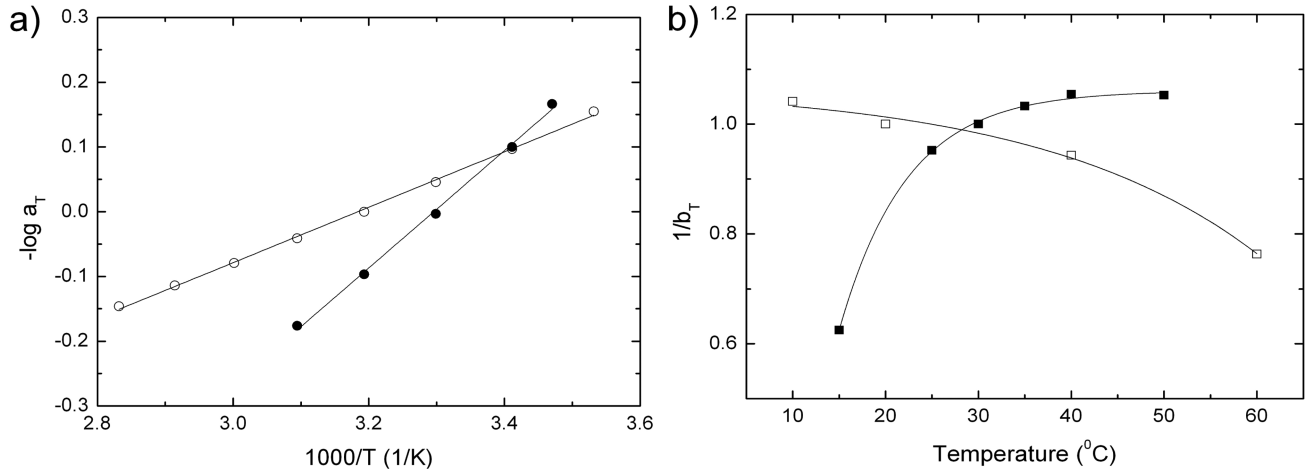

Figure 10. (a) Arrhenius plot for scaling parameter a_T for copolymer $BO_{14}EO_{378}BO_{14}$ at 6 (○) and 10 (●) wt %. (b) Temperature dependence of $1/b_T$ for copolymer $BO_{21}EO_{385}BO_{21}$ at 5 (■) and 10 (□) wt % solutions.

boundary can be assigned as defective versions of cubic-packed gels as mentioned previously; they are characterized by a constant value of G', the shallow minimum in G'', and both moduli do not show a crossover point in the measured frequency range as observed in Figure 8d. Nevertheless, the G' values for the viscous fluid are much lower compared to those of a pure gel phase, which well-exceeded 1 kPa and possessed the characteristic features of immobile gels constituted by cubic packing of spherical micelles completely independent of temperature and frequency.[39] The plateau behavior of G' and the minimum in G'' have been also observed for colloidal hard spheres near the glass-fluid transition[40] and is also characteristic of the cubic phase in block copolymer melts.[41] The frequency-independent regime took place at lower concentrations for copolymer $BO_{21}EO_{385}BO_{21}$ than for $BO_{14}EO_{378}BO_{14}$, due to its larger hydrophobicity, which favored both micellization and micellar bridging due to the longer BO blocks.

Plots of G' and G'' versus frequency presented in Figure 8 then show a wide variety of viscoelastic characteristics from purely viscous to highly elastic. This behavior confirms the formation of a dynamic network, which becomes more robust as the concentration is increased as also observed for other $BO_mEO_nBO_m$ copolymers as $BO_{12}EO_{114}BO_{12}$,[23] $BO_{12}EO_{227}BO_{12}$,[32] and $BO_{10}EO_{227}BO_{10}$.[29] Apart from the direct visual observations of certain chain cross-linking between micelles by AFM, the emergence of slow relaxation processes as the concentration increased in the dilute regime (<4 wt %) also corroborates the existence of this dynamic network. The contribution of micelle packing as effective hard spheres in the gel phase to the rheological response became predominant at larger concentrations for which G' became frequency-independent. Nevertheless, the effect of bridging was still observed, notably upon the slow relaxation after shearing when compared to the fast relaxation of micellar solutions of nonbridging spherical micelles. Also, $BO_{14}EO_{378}BO_{14}$ and $BO_{21}EO_{385}BO_{21}$ copolymers did not behave as classical colloidal suspensions interacting through weak short-range attractive forces, in which G' is frequency-independent and increases with concentration and G'' is concentration-independent and increases linearly with frequency. These facts allow one to scale the moduli against frequency to give smooth master curves[42] (see below).

Hence, $BO_{14}EO_{378}BO_{14}$ and $BO_{21}EO_{385}BO_{21}$ denote a more complex rheology as observed from frequency scans, which also impeded to fit their behavior to that of a Maxwell fluid. Strikingly, this behavior was rather different to that observed for other structurally very related copolymer, $BO_{10}EO_{410}BO_{10}$. For this copolymer, typical values of G'' exceed those of G' over a similar accessible frequency range, as also observed for other classical associative thickeners such as $C_nUEO_mUC_n$ and $C_nEO_mC_n$ polymers (C = methylene unit and U = urethane linkage via an isophoronediisocyanate residue),[43] whose

dx.doi.org/10.1021/jp500426k | J. Phys. Chem. B XXXX, XXX, XXX−XXX

lengthy EO and C blocks can be modeled by a single Maxwell element. Despite the similar EO length and larger BO blocks compared with $BO_{10}EO_{410}BO_{10}$, the larger polydispersities of $BO_{14}EO_{378}BO_{14}$ and $BO_{21}EO_{385}BO_{21}$ can broaden the Poisson distribution of BO block-lengths (assuming ideal polymerization).[44] The larger distribution of hydrophobic-block lengths implies a wider temperature range for micellization, with the full associative thickening effect being developed only when the extent of micellization and, consequently, the extent of bridging is high; that is, the present copolymers effectively behave as having lower effective BO block lengths having a behavior closer to $BO_{12}EO_{114}BO_{12}$, $BO_{10}EO_{227}BO_{10}$, or $BO_{10}EO_{227}BO_{10}$ copolymers.

3.4.5. Scaling of Rheological Response. To additionally evaluate the mechanical response of copolymers $BO_{14}EO_{378}BO_{14}$ and $BO_{21}EO_{385}BO_{21}$ the construction of a master curve through the time−temperature superposition of the measured moduli was performed in order to facilitate the comparison of the frequency response at different temperatures. The moduli and the frequencies for each data set were independently scaled by factors a_T and b_T, respectively, to obtain a superposition of G' and G''. The temperature dependence of the moduli was explored for 6 and 10 wt % solutions in the range of 5−70 °C as examples (i.e., corresponding to the immobile gel phase for copolymers $BO_{14}EO_{378}BO_{14}$ and $BO_{21}EO_{385}BO_{21}$) (Figure 9). The data suggested that there were no changes in the nature of the dynamic mechanical response in the gel phase as a function of temperature in the range of 10−50 °C. As commented previously, the independence of G' with frequency and the minimum in G'' in the gel phase region were, in part, the result of the formation of a cubic mesophase similar as that observed in hard sphere suspensions under shear near the fluid−glass transition. However, the shrinkage of the micellar corona at relatively high temperatures can lead to defects in micellar packing and the bridged network, which might well change the scaling of the viscoelastic behavior with frequency within the hard gel phase.

The Arrhenius plot of $-\log(a_T)$ against $1/T$ (Figure 10a), which has a slope equivalent to a plot of log(relaxation rate) against $1/T$, gave mean activation energy values, E, of −17 and −50 kJ mol^{-1} for copolymers $BO_{14}EO_{378}BO_{14}$ and $BO_{21}EO_{385}BO_{21}$, respectively, as an average value over all components of the copolymer solutions. The lower (more negative) E value for $BO_{21}EO_{385}BO_{21}$ is in agreement with harder gels, resulting from a more hydrophobic copolymer. The plot of $1/b_T$ against T shown in Figure 10b indicates an increase in the high-frequency storage modulus with temperature in the interval from 10 to 50 °C for the 5 wt % solution, with the dependence of G' on T being much greater than that predicted by the kinetic theory of network elasticity for a fully formed network; conversely, at 10 wt %, the behavior is the opposite, in agreement with the shrinkage of the cubic mesoscopic structure of packed micelles.

The negative values of the activation energy for the relaxation process found for solutions of the present copolymers were similar to those previously found for copolymer $BO_{10}EO_{410}BO_{10}$, and are in great contrast to positive values (E = from +30 to +70 kJ mol^{-1}) measured for solutions of other associative thickeners such as $C_nUEO_mUC_n$ and $C_nEO_mC_n$ copolymers;[43,45,46] that is, the relaxation times for $BO_{14}EO_{378}BO_{14}$ and $BO_{21}EO_{385}BO_{21}$ solutions increased with increasing temperature, whereas those for $C_nUEO_mUC_n$ and $C_nEO_mC_n$ solutions decreased with increasing temperatures. Hence, for the present copolymers, the activation energy might involve both the disengagement of chain ends from micelles (a positive contribution) and micellization (a negative one) in contrast to alkyl-ended copolymer solutions, where only disengagement is important provided that their extent of micellization is low over the temperature range of interest. For both $BO_{14}EO_{378}BO_{14}$ and $BO_{21}EO_{385}BO_{21}$ copolymers micellization is the dominant process and increases as temperature does. The increase of the high-frequency G' modulus with increasing T is consistent with this explanation. For solutions of classical associative thickeners, copolymers $C_nUE_mUC_n$ and $C_nE_mC_n$, the high frequency storage modulus is either weakly sensitive to temperature ($C_{16}U$ or C_{20})[43,45,47] or falls with increasing temperature ($C_{12}U$ or C_{16}).[46] The fall has been ascribed as temperature is increased to an enhanced tendency for the copolymers to loop in a single micelle rather than to bridge between micelles. Hence, at first, it could be thought that there is a contradiction between our assumptions that $BO_{14}EO_{378}BO_{14}$ and $BO_{21}EO_{385}BO_{21}$ copolymers are fully micellized at room temperature in dilute solution (0.1−1 wt %, see Micellar Properties) but not in a concentrated solution (>4 wt %). However, it is known[48] that the micelle-unimer equilibrium changes dramatically when the concentration of copolymer is increased (i.e., when the H-bonded structure of water and, hence, the hydrophobic effect that drives micellization is greatly reduced).[49] The effect of mass action is opposed by this reduction in the hydrophobic effect, and in a gel solution, the shorter BO blocks are less likely to enter micelles than in a 1 wt % solution, which is favored by the broader Poisson BO block distributions.

4. CONCLUSIONS

In summary, in this work the self-assembly and physical properties of reverse triblock copolymers $BO_{14}EO_{378}BO_{14}$ and $BO_{21}EO_{385}BO_{21}$ have benn analyzed in detail. These block copolymers form swollen flowerlike micelles 20 to 40 nm in size as observed from DLS, which can be interconnected to a certain extent in the form of micellar clusters in the very dilute regime as observed by AFM imaging. As a result of their long BO blocks and extremely lengthy EO ones, these two copolymers also exhibited a very rich phase behavior, modulated from an unstructured fluid to a gel only by changing the solution temperature, concentration, and/or by the application of an external stress. A wide variety of viscoelastic characteristics from purely viscous to highly elastic were observed from frequency scans. The presence of micellar bridging could be additionally confirmed by the observation of a slow relaxation of the gel network under the application of an external stress. In general, the behavior of both $BO_{14}EO_{378}BO_{14}$ and $BO_{21}EO_{385}BO_{21}$ behavior was rather different to that observed for another structurally similar copolymer, $BO_{10}EO_{410}BO_{10}$, for which typical values of G'' exceed those of G' over a similar accessible frequency range, as also observed for other classical associative thickeners such as $C_nUEO_mUC_n$ and $C_nEO_mC_n$ polymers.[15] The larger polydispersities of $BO_{14}EO_{378}BO_{14}$ and $BO_{21}EO_{385}BO_{21}$ can broaden the Poisson distribution of BO block-lengths (assuming ideal polymerization)[44] to account for these differences, making these copolymers behave as having lower effective BO block lengths having a behavior closer to $BO_{12}EO_{114}BO_{12}$,[23] $BO_{12}EO_{227}BO_{12}$,[32] or $BO_{10}EO_{227}BO_{10}$[29] copolymers. This effect is reflected in the negative values of the activation energy

dx.doi.org/10.1021/jp500426k | J. Phys. Chem. B XXXX, XXX, XXX−XXX

derived from master curves, which denoted both the disengagement of chain ends from micelles (a positive contribution) and the predominant micellization (a negative one), in contrast to the positive values observed for classical associative thickeners.[15]

The absence of transfer reaction during copolymerization, the larger hydrophobicity of the BO block compared that of the PO block (six time larger), and the wide range of copolymeric species observed, from single micelles to micellar clusters to viscous fluids and gels, make the present $BO_{14}EO_{378}BO_{14}$ and $BO_{21}EO_{385}BO_{21}$ copolymers a very interesting alternative to Pluronic copolymers for constructing nanosized carriers for drug transport and release. In particular, depending on the species and the desired disease to treat different administration routes might be envisaged as, for example, parenteral (micelles), oral (micellar clusters), and/or subdermal and topical administration (gel depots) using much lower polymer concentrations, loading much higher drug contents, and being more physiologically stable than Pluronics. In fact, these copolymers have been already tested to carry and deliver the anticancer drug doxorubicin with a smooth release rate to cancerous cells with great success.[25] In addition, the creation of hydrophobic domains by the observed micellar entanglement might be the origin of the enhanced interaction of the present copolymers with cellular membranes and, in particular, by largely decreasing the activity of the poly(glycol)protein-P (pg-P) efflux pump in multidrug resistant cells, favoring drug accumulation inside the cells.[50] However, more detailed studies are required to establish exact correlations between copolymer structure, copolymers solution behavior, polymer/cell interactions, and the mechanisms by which the cellular responses are drastically modified.

AUTHOR INFORMATION

Corresponding Author

*E-mail: silvia.barbosa@usc.es.

Author Contributions

‖These authors contributed equally to this work.

Notes

The authors declare no competing financial interest.

ACKNOWLEDGMENTS

Authors thank Ministerio de Economía y Competitividad (MINECO) for the research project MAT 2010-17336, Xunta de Galicia for research grants CN2012/072 and EM2013-046. S.B. also thanks MINECO for her Ramón y Cajal fellowship. The authors specially thank Prof. D. Attwood and Prof. C. Booth for generous gifts of copolymer samples.

REFERENCES

(1) Farokhzad, O. C.; Langer, R. *Adv. Drug Delivery Rev.* **2006**, *58*, 1456−1459.
(2) Cho, K.; Wang, X.; Nie, S.; Chen, Z.; Shin, D. M. *Clin. Cancer Res.* **2008**, *14*, 1310−1316.
(3) Arias, J. L. *Mini-Rev. Med. Chem.* **2011**, *11*, 1−17.
(4) Lee, P. Y.; Wong, K. K. Y. *Curr. Drug Delivery* **2011**, *8*, 245−253.
(5) Heidel, J.; Davis, M. *Pharm. Res.* **2011**, *28*, 187−199.
(6) Chu, B. *Langmuir* **1995**, *11*, 414−421.
(7) Kabanov, A. V.; Alakhov, V. Y. *Crit. Rev. Ther. Drug Carrier Syst.* **2002**, *19*, 1−72.
(8) Batrakova, E. V.; Kabanov, A. V. *J. Controlled Release* **2008**, *130*, 98−106.
(9) Alvarez-Lorenzo, C.; Sosnik, A.; Concheiro, A. *Curr. Drug Targets* **2011**, *12*, 1112−1130.
(10) Yu, G.-E.; Masters, A. J.; Heatley, F.; Booth, C.; Blease, T. G. *Macromol. Chem. Phys.* **1994**, *195*, 1517−1538.
(11) Yu, G.-E.; Altinok, H.; Nixon, S. K.; Booth, C.; Alexandridis, P.; Hatton, T. A. *Eur. Polym. J.* **1997**, *33*, 673−677.
(12) Mortensen, K.; Batsberg, W.; Hvidt, S. *Macromolecules* **2008**, *41*, 1720−1727.
(13) Booth, C.; Attwood, D. *Macromol. Rapid Commun.* **2000**, *21*, 501−527.
(14) Taboada, P.; Velasquez, G.; Barbosa, S.; Castelletto, V.; Nixon, S. K.; Yang, Z.; heatley, F.; Hamley, I. W.; Ashford, M.; Mosquera, V.; Attwood, D.; Booth, C. *Langmuir* **2005**, *21*, 5263−5271.
(15) Taboada, P.; Velasquez, G.; Barbosa, S.; Yang, Z.; Nixon, S. K.; Zhou, Z.; Heatley, F.; Ashford, M.; Mosquera, V.; Attwood, D.; Booth, C. *Langmuir* **2006**, *22*, 7465−7470.
(16) Booth, C.; Attwood, D.; Price, C. *Phys. Chem. Chem. Phys.* **2006**, *8*, 3612−3622.
(17) Barbosa, S.; Cheema, M. A.; Taboada, P.; Mosquera, V. *J. Phys. Chem. B* **2007**, *111*, 10920−10928.
(18) Crothers, M.; Zhou, Z.; Ricardo, N. M. P. S.; Yang, Z.; Taboada, P.; Chaibundit, C.; Attwood, D.; Booth, C. *Int. J. Pharm.* **2005**, *293*, 91−100.
(19) Ribeiro, M. E. N. P.; de Oliverira, S. M.; Ricardo, N. M. P. S.; Mai, S.-M.; Attwood, D.; Yeates, S. G.; Booth, C. *Int. J. Pharm.* **2008**, *362*, 193−196.
(20) Heatley, F.; Yu, G.-e.; Sun, W.-B.; ywell, J.; Mobbs, R. H.; Booth, C. *Eur. Polym. J.* **1990**, *26*, 583−592.
(21) Yu, G.-e.; Yang, Z.; Ameri, M.; Attwood, D.; Collett, J. H.; Price, C.; Booth, C. *J. Phys. Chem. B* **1997**, *101*, 4394−4401.
(22) Mistry, D.; Annable, T.; Yuan, X.-F.; Booth, C. *Langmuir* **2006**, *22*, 2986−2992.
(23) Kelarakis, A.; Yuan, X.-F.; Mai, S.-M.; Yang, Y.-W.; Cooth, C. *Phys. Chem. Chem. Phys.* **2003**, *5*, 2628−2634.
(24) Zhou, Z.; Yang, Y.-W.; Booth, C.; Chu, B. *Macromolecules* **1996**, *29*, 8357−8361.
(25) Cambón, A.; Rey-Rico, A.; Mistry, D.; Brea, J.; Loza, M. I.; Attwood, D.; Barbosa, S.; Alvarez-Lorenzo, C.; Concheiro, A.; Taboada, P.; Mosquera, V. *Int. J. Pharm.* **2013**, *445*, 47−57.
(26) Yang, Y.-W.; Yang, Z.; Zhou, Z.-K.; Attwood, D.; Booth, C. *Macromolecules* **1996**, *29*, 670−680.
(27) Cambón, A.; Alatorre-Meda, M.; Juárez, J.; Topete, A.; Mistry, D.; Attwood, D.; Barbosa, S.; Taboada, P.; Mosquera, V. *J. Colloid Interface Sci.* **2011**, *361*, 154−158.
(28) Provencher, S. W. *Die Makromolekulare Chemie* **1979**, *180*, 201−209.
(29) Kelarakis, A.; Ming, X.-T.; Yuan, X.-F.; Booth, C. *Langmuir* **2004**, *20*, 2036−2038.
(30) Castelletto, V.; Hamley, I. W.; Yuan, X.-F.; Kelarakis, A.; Booth, C. *Soft Matter* **2005**, *1*, 138−145.
(31) Liu, T.; Nace, V. M.; Chu, B. *J. Phys. Chem. B* **1997**, *101*, 8074−8078.
(32) Kelarakis, A.; Havredaki, V.; Yuan, X.-F.; Chaibundit, C.; Booth, C. *Macromol. Chem. Phys.* **2006**, *207*, 903−909.
(33) Cambón, A.; Barbosa, S.; Rey-Rico, A.; Figueroa-Ochoa, E. B.; Soltero, J. F. A.; Yeates, S. G.; Alvarez-Lorenzo, C.; Concheiro, A.; Taboada, P.; Mosquera, V. *J. Colloid Interface Sci.* **2012**, *387*, 275−284.
(34) Liu, T.; Zhou, Z.; Wu, C.; Nace, V. M.; Chu, B. *J. Phys. Chem. B* **1998**, *102*, 2875−2882.
(35) Hvidt, S.; Joergensen, E. B.; Brown, W.; Schillen, K. *J. Phys. Chem.* **1994**, *98*, 12320−12328.
(36) Prud'homme, R. K.; Wu, G.; Schneider, D. K. *Langmuir* **1996**, *12*, 4651−4659.
(37) Hamley, I. W.; Mai, S.-M.; Ryan, A. J.; Fairclough, P. A.; Booth, C. *Phys. Chem. Chem. Phys.* **2001**, *3*, 2972−2980.
(38) Li, H.; Yu, G.-E.; Price, C.; Booth, C. *Macromolecules* **1997**, *30*, 1347−1354.
(39) Juárez, J.; Taboada, P.; Valdez, M. A.; Mosquera, V. *Langmuir* **2008**, *24*, 7107−7116.

(40) Mason, T. G.; Weitz, D. A. *Phys. Rev. Lett.* **1995**, *75*, 2770−2773.
(41) Zhao, J.; Majumdar, B.; Schulz, M. F.; Bates, F. S. *Macromolecules* **1996**, *29*, 1204−1215.
(42) Trappe, V.; Weitz, D. A. *Phys. Rev. Lett.* **2000**, *85*, 449−452.
(43) Annable, T.; Buscall, R.; Ettelaie, R. *Colloids Surf., A* **1996**, *112*, 97−116.
(44) Flory, P. J. *Principles of Polymer Chemistry*; Cornell University Press: Ithaca, 1953.
(45) Alexandridis, P.; Lindman, B. *Amphiphilic Block Copolymers. Self-Assembly and Applications*; Elsevier: Amsterdam, 2000.
(46) Mistry, D. Block copolymers for use as associative thickeners. Ph.D. Thesis, University of Manchester: Manchester, UK. 2000.
(47) Annable, T.; Buscall, R.; Ettelaie, R.; Whittlestone, D. *J. Rheol.* **1993**, *37*, 695−726.
(48) Nixon, S. K.; Hvidt, S.; Booth, C. *J. Colloid Interface Sci.* **2004**, *280*, 219−223.
(49) Tanford, C. *The Hydrophobic Effect*; Wiley: New York, 1980.
(50) Cambón, A.; Brea, J.; Loza, M. I.; Alvarez-Lorenzo, C.; Concheiro, A.; Barbosa, S.; Taboada, P.; Mosquera, V. *Mol. Pharm.* **2013**, *10*, 3232−3241.